Scientific report; WR 95-05

Ministerie van Verkeer en Waterstaat
Koninklijk Nederlands Meteorologisch Instituut
in cooperation with
Utrecht University,
Department of Mathematics

Numerical studies on the Lorenz-84 atmosphere model

Leonardo Anastassiades

De Bilt, 1995

Scientific report; WR 95-05

De Bilt, 1995

Postbus 201
3730 AE De Bilt
the Netherlands
Telephone 030-206 911
Telefax 030-210 407

(after 10-10-'95
tel. +31(0)30-22 06 911
fax +31(0)30-22 10 407)

UDC: 167.7.001.573
551.511.6
551.58
ISSN: 0169-1651
ISBN: 90-369-2077-9

Numerical Studies on the

Lorenz-84

Atmosphere Model

Studienarbeit

By cand. ing. Anastassiades Leonardo

at the Department of Mathematics
of the Utrecht University

and the Royal Netherlands Meteorological Institute (KNMI)

Supervisors: Prof. Dr. F. Verhulst and Dr. J.D. Opsteegh

For this work I want to thank my supervisors Prof. F. Verhulst of the Department of Mathematics of the University of Utrecht and Dr. T. Opsteegh of the Royal Institute of Meteorology Netherlands (KNMI) for their excellent supervision of my work. I also thank Prof. A. Kistner of the Institute A for Mechanics of the Stuttgart University who encouraged me to do this work abroad. My special thanks go also to the researching group (Voorspelbaarheidsgroep) of the Royal Dutch Meteorological Institute (KNMI) and especially Frank Selten for helping in programming the graphical routines of my bifurcation analysis program and whose Lyapunov exponent program I used. Also to Dr. Arjen Doelman of the Mathematical Department of the Utrecht University who gave me precious mathematical advices in my investigations and who helped me to correct this paper. Not to forget, I thank Dr. Gert van der Heijden working at the Center for Nonlinear Dynamics of the London University College who gave me his programs for determining the Lyapunov exponent and the Correlation dimension of attractors and for the good advice he gave me in investigating my dynamical system.

Last but not least, my thanks are also going to my family, who supported me in every way during my studies and to Maryline to whom I dedicate this work.

Contents

Chapter 1

Introduction

In this work we do the first part of a meteorological project running in the Royal Netherlands Meteorological Institute (KNMI) in cooperation with the Department of Mathematics of the University of Utrecht, by investigating an autonomous low order atmosphere model introduced by E.N. Lorenz, [3] and [6]. We hope that this work will clarify in a way the picture of the Lorenz-84 model which is still poorly investigated and show some of the various interesting phenomena of the system.

The analysis of the system is necessary in order to be able to develop a coupled atmosphere-ocean model with behaviour that mimics as close as possible the behaviour of the real climate system. This means that the atmospheric model must exhibit chaotic behaviour for a range of parametervalues.

Chapter 2

An Atmosphere Model

2.1 Equations of the Lorenz-84 Model

A system describing the large scale atmospheric circulation can be modeled, according to [3] with a nonlinear system of three coupled ordinary differential equations.

The equations of this low-order atmospheric model are given in [3] and [6] by:

$$\dot{X} = -Y^2 - Z^2 - aX + aF \tag{2.1}$$

$$\dot{Y} = XY - bXZ - Y + G \tag{2.2}$$

$$\dot{Z} = bXY + XZ - Z \tag{2.3}$$

The independent variable t represents time. The variable X represents the strength of a large-scale westerly-wind current zonal flow (equivalent to the meridional temperature gradient). The variables Y and Z represent the amplitudes of the cosine and sine phases of a chain of large scale superposed waves. The parameter F in eq. (2.1) represents a forcing of the westerly current, due to the north-south temperature gradient, while G in eq. (2.2) represents a forcing by the continent-ocean temperature contrast. The quadratic

terms $-bXZ$ and bXY in eq. (2.2) and (2.3) respectively represent the translation of the waves by the westerly current.

The quadratic terms $-Y^2$ and $-Z^2$ in eq. (2.1), XY and XZ in eq. (2.2) and (2.3) represent a transfer of energy, from the westerly current to the waves.

The linear terms $-aX$, $-Y$ and $-Z$ take energy out of the system, and represent thermal and mechanical damping.

In this study we will abbreviate the system given by the equations (2.1)-(2.3) with:

$$\dot{\underline{x}} = \underline{f}(\underline{x}); \quad \underline{x}(0) = \underline{x}_0 \quad \text{where} \quad \underline{x} \in \mathrm{R}^3 \tag{2.4}$$

Here $\underline{x}$ is the vector of the variables X,Y,Z, $\underline{f}(\underline{x})$ is a nonlinear vector function and $\underline{x}_0$ is the initial condition.

Chapter 3

Numerical investigations

3.1 Qualitative behaviour of the system

By equating eq. (2.1) to zero we get the equation of the surface on which the passing through trajectories have a tangent vector parallel to the Y - Z plane. This is given by:

$$X = F - \frac{Y^2}{a} - \frac{Z^2}{a}, \tag{3.1}$$

and represents a paraboloid with symmetry axis X and top at $X = F$. The paraboloid is illustrated in fig. 3.1.

Outside of the paraboloid the time derivative $\dot{X}$ is negative. This happens for example when X is larger than F. So the X variable decreases. Inside the time derivative $\dot{X}$ is positive, and X increases. In fig. 3.1 we show this behaviour with arrows inside and outside the paraboloid.

The intersection of the paraboloid with the $X-Y$ plane and the vector field of the system on this plane, described by eq. (2.1) and (2.2) for $a = 0.25$, $b = 4$, $F = 9.0$, $G = 0.0$ are illustrated in fig. 3.2. The solid line in fig. 3.2 with the number 2 on its top is the isoline where $\dot{X} = 2.0$. The solid line with the number 0 is the intersection of the paraboloid with the $X - Y$ plane. The dashed

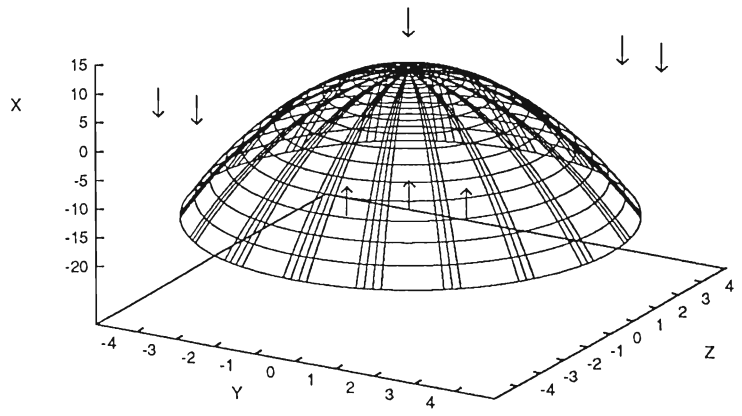

Figure 3.1: The paraboloid surface where the vector field is tangent to $Y-Z$ plane for $F = 9$.

lines correspond to negative strength isolines $\dot{X} = -2, -4, -6, \ldots, -14$. So the qualitative behaviour of the system is that the solutions are bounded in the X-direction under the top of the paraboloid. Seeing this picture one can imagine a circulation of the system going downwards when the trajectories come out of the paraboloid and going up from the moment they enter the paraboloid in lower values of X. This behaviour shows up in the case of a strange attractor later in this section.

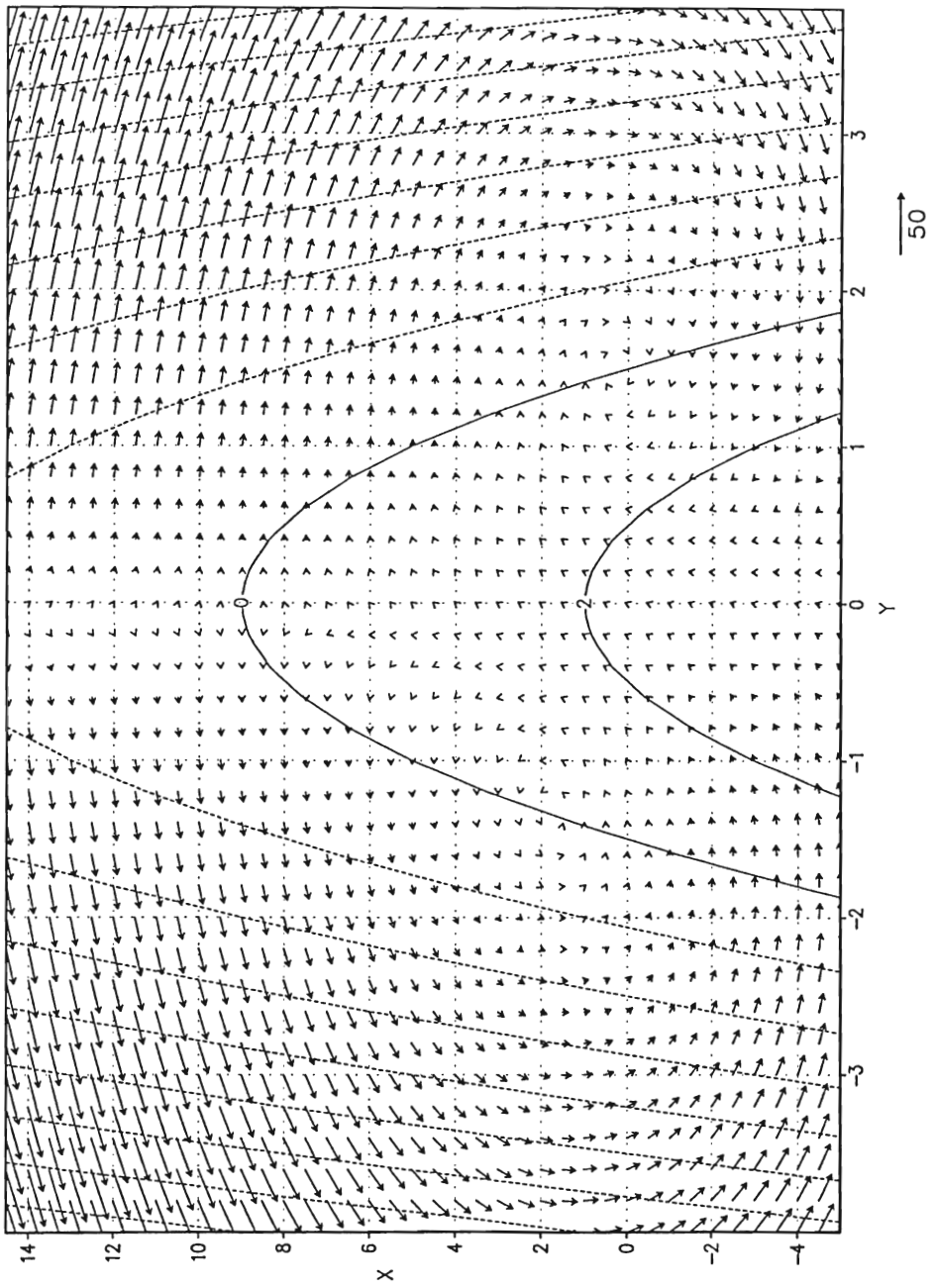

Figure 3.2: The parabola of the paraboloid surface where the vector field is tangent to $Y - Z$ plane has on its top the number 0.

As we can observe by numerical time integrations for different parameters the system comes to a chaotic region when there is a relatively large temperature gradient between the polar and equatorial zones. For small forcing the behaviour is regular and we get fixed points and limitcycles.

In fig. 3.3 a colour picture of a strange attractor is illustrated. Here the trajectory in state-space is drawn, after the transient motion has dissapeared.

The trajectory changes colour according to the absolute value of the westerly wind $\dot{X}$ acceleration. The colours choosen are mapped in the form of the rainbow spectrum. Beginning with black which is the maximum acceleration we go through the colours dark blue, blue, green, yellow, orange, red violet to acceleration zero.

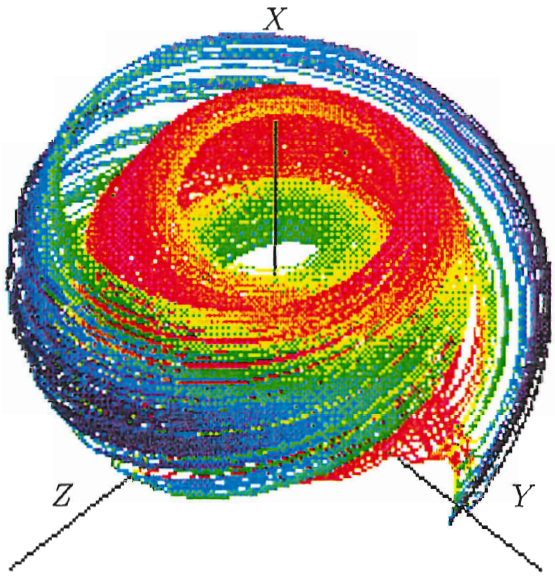

Figure 3.3: A strange attractor for $a = 0.25$, $b = 4.0$, $F = 8.0$, $G = 1.0$, $X_0 = 2.4$, $Y_0 = 1.0$, $Z_0 = 0.0$.

With this picture we can very well see and qualitatively estimate the timescales of some interesting processes.

- The energy gain of the westerly wind X by the forcing F,
- the transfer of energy to the superposed waves Y and Z, taking place when X comes to large values,
- the dissipation process influencing the Y and Z values taking place when X has no more energy to give.

If we take into account that the trajectories travel clockwise arround the X axis we can see that near the violet area just over the top of the X-axis we have almost no westerly wind acceleration. This area is also the top of the paraboloid, fig. 3.1.

From this moment the energy transport takes the major role. Very fast, approximately proportional to $Y^2 + Z^2$ (which is the squared vertical distance of the trajectory from the X axis) X looses its energy. About halfway downwards of the attractor we have the maximum deceleration of X. There the colour is dark-blue to black.

As X has no more energy to give and the attractors distance from the X-axis is at about its maximum, the deceleration of X becomes weaker changing from blue to green and yellow. Now the dissipation process begins to take place. This process is rather slow, and the trajectory approaches the X axis.

For very small values of Y and Z equations (2.1) to (2.3) can be approximated by:

$$\dot{X} \approx -aX + aF \tag{3.2}$$

$$\dot{Y} \approx -Y + G \tag{3.3}$$

$$\dot{Z} \approx -Z \tag{3.4}$$

So the system starts getting energy from the forcing F with a rate approximately proportional to the difference of $F - X$ and the trajectory spirals it

self up again to the area where we started. Halfway upwards it has about the acceleration corresponding to the yellow colour.

From eq. (2.1) we can see that X can gain energy only by the thermal forcing F. All the other terms on the right hand side of this equation try to damp this quantity.

3.2 Numerical integration methods

We used two numerical integration schemes to integrate the system in time. The first is a Runge-Kutta integration scheme with fixed time steps with a local error of $O(h^4)$ [16]. The second is a Runge-Kutta-Fehlberg integration scheme with fixed or automatically controlled time steps. The latter has a local error of $O(h^5)$. As the results with both integration schemes reproduce each other we will give in this study only the results of the Runge-Kutta scheme.

3.3 The Poincaré section

A useful way to visualize a chaotic attractor is the Poincaré section [10], [14].

We know that the variables Y and Z describe a traveling wave. Thus the trajectories in the X,Y,Z space tend to rotate about the X-axis. This rotational behavior we have already seen in fig. 3.3 were the trajectory moves in clockwise direction around the X-axis. Somebody could simply take the $Y = 0$ and the $Z = 0$ plane as the penetration plane for our Poincaré sections.

Two Poincaré sections, one with $Y = 0$ and one with the $Z = 0$ plane corresponding to the chaotic attractor in fig. 3.3 are given in fig. 3.4. The parameters used are taken from [6].

We got these Poincaré sections by marking every point of the trajectory passing the $Y = 0$ and the $Z = 0$ plane respectively. So we have ploted the

penetration points in the **in** and **out** direction. Note that the pattern (figure 3.4) is typical for chaotical systems and indicates the fractal structure of the attractor.

Very interesting to see in see picture 3.4 (a), is that the Poincaré section of **one single trajectory** consists of three domains. Since a chaotic attractor has no periodicity the points never repeat and the structure gets denser and denser as integration time grows but without changing the shape seen in the picture. In order to understand these Poincaré sections better, we show in

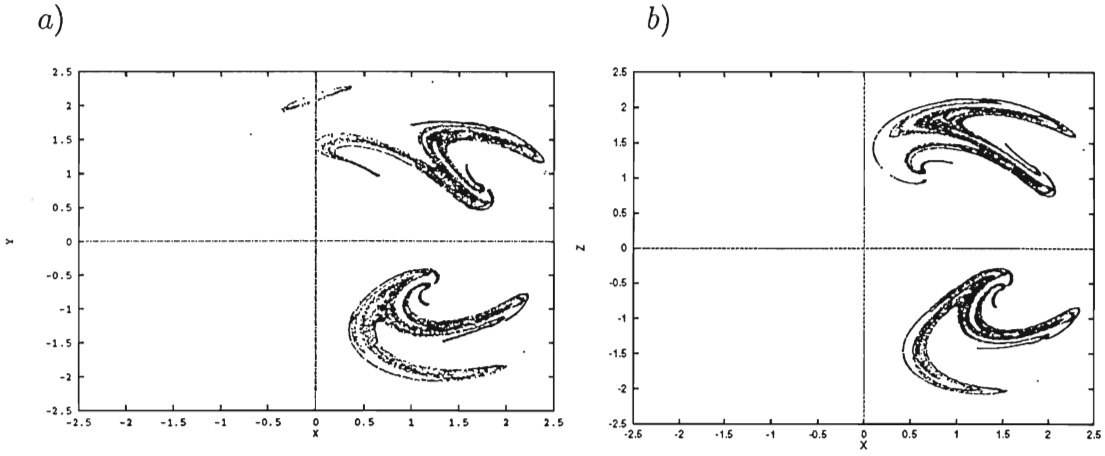

Figure 3.4: Poincaré section of a strange attractor for $a = 0.25$, $b = 4.0$, $F = 8.0$, $G = 1.0$, $X_0 = 2.4$, $Y_0 = 1.0$, $Z_0 = 0.0$. a) intersection with the Z=0 plane, b) intersection with the Y=0 plane.

fig. 3.5 the YZ-projection of the phase portrait of the strange attractor. Paying attention at the places where the trajectory crosses the axis and at the density of the lines there, we can qualitatively see the relation to fig. 3.4. For larger positive values of Y we also see that the trajectory crosses the Z axis rarely. The intersection points correspond to the small isolated pattern we get on the top of fig. 3.4 (a).

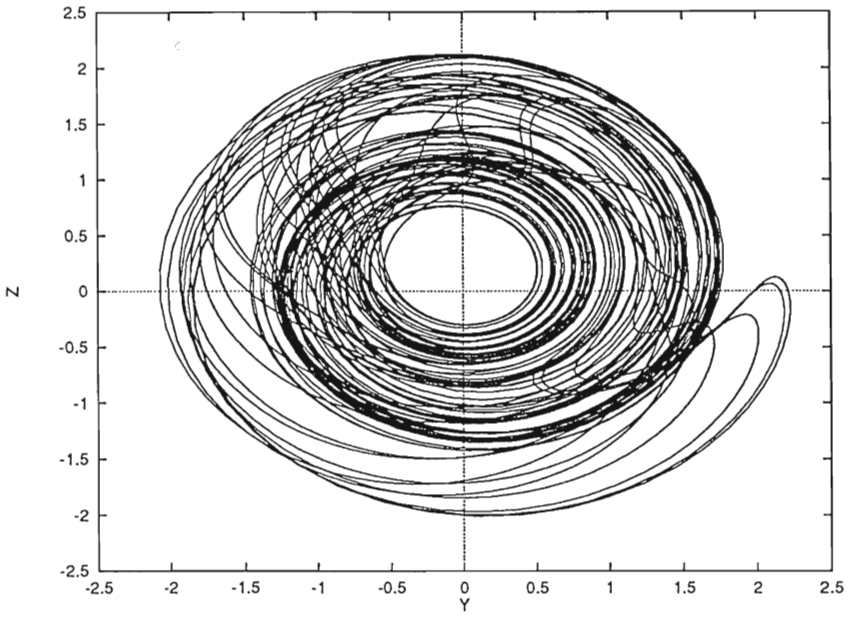

Figure 3.5: The YZ-projection of the phase portrait of the strange attractor: $a = 0.25$, $b = 4.0$, $F = 8.0$, $G = 1.0$, $X_0 = 2.4$, $Y_0 = 1.0$, $Z_0 = 0.0$.

3.4 Bifurcation analysis of the equilibrium solutions

3.4.1 The equilibrium solutions and their stability behaviour

We first consider the steady-state solutions of eq. (2.4). Equating the time derivative to zero they are given by:

$$\underline{f}(\underline{x}) = 0. \tag{3.5}$$

It can be shown that the steady-state solution are given by the equations:

$$a(F - X)(1 - 2X + (1 + b^2)X^2) - G^2 = 0 \tag{3.6}$$

$$Y = \frac{(1-X)G}{(1-2X+(1+b^2)X^2)} \tag{3.7}$$

$$Z = \frac{bXG}{(1-2X+(1+b^2)X^2)} \tag{3.8}$$

Eq. (3.6) is a polynomial of order 3 in X with real coefficients. So there are two possibilities of solutions of X for a given set of parameters a, b, F and G. The first possibility is three real solutions. The second is one real and two conjugate complex solutions for X.

A simple way to solve the above system of algebraic equations without even solving the cubic, is to give values of X and F and calculate G from eq. (3.6) [3].

If we rewrite eq. (3.6) in the form:

$$G = \pm\sqrt{a(F-X)((1-X)^2+b^2X^2)} \tag{3.9}$$

we see that there exist two real solutions of G of the same value but opposite sign.

Denoting that the term

$$((1-X)^2+b^2X^2)$$

on the right hand side of eq. (3.9) is always positive we see that real solutions are only possible for X smaller than F.

Since in eq. (3.7) and (3.8) G is found to be a factor in front of expressions in X there exists a symmetry in the steady state solution about the $X-F$-plane so that each equilibrium point: X, Y, Z, G, F has a symmetrical equilibrium solution $X, -Y, -Z, -G, F$.

We can linearize our system (2.4) at an arbitrary equilibrium point as follows:

$$\dot{\underline{\xi}} = J_e\underline{\xi}$$

where $\underline{\xi} = \underline{x} - \underline{x}_e$ and $J = \frac{\partial \underline{f}}{\partial \underline{x}}$ is the Jacobian matrix at the equilibrium point. The index e denotes the equilibrium point. Our system has the Jacobian matrix:

$$J = \begin{pmatrix} -a & -2Y & -2Z \\ Y - bZ & X - 1 & -bX \\ bY + Z & bX & X - 1 \end{pmatrix} \tag{3.10}$$

The matrix is real, nonsymmetric and of order three.

The eigenvalue problem for the linearized system at an arbitrary equilibrium point, leads us to the following equation:

$$|J - sI| = 0. \tag{3.11}$$

where s denotes the eigenvalues and I is the unitary matrix. Calculating the left hand side of eq. (3.11) we get the characteristic equation which is in our case of third order in s. Again we can say that two types of eigenvalues are possible:

- Three real eigenvalues or
- One real and two conjugate complex.

Similar to the symmetry of the equilibrium solution to the F-X plane, we have also symmetry of the stability behaviour of the system to the same plane.

That means that the equilibrium solution X, Y, Z, F, G has the same stability behaviour as the equilibrium solution $X, -Y, -Z, F, -G$. This can be shown very easily: If :

$$J = \begin{pmatrix} -a & -2Y & -2Z \\ Y - bZ & X - 1 & -bX \\ bY + Z & bX & X - 1 \end{pmatrix}$$

is the Jacobian of the system at the fixed point X, Y, Z, F, G then:

$$J^{-} = \begin{pmatrix} -a & 2Y & 2Z \\ -Y + bZ & X - 1 & -bX \\ -bY - Z & bX & X - 1 \end{pmatrix}$$

is the Jacobian for the fixed point $X, -Y, -Z, F, -G$.

It can be shown that:

$$\begin{vmatrix} a_{11} & a_{12} & a_{13} \\ a_{21} & a_{22} & a_{23} \\ a_{31} & a_{32} & a_{33} \end{vmatrix} = \begin{vmatrix} a_{11} & -a_{12} & -a_{13} \\ -a_{21} & a_{22} & a_{23} \\ -a_{31} & a_{32} & a_{33} \end{vmatrix}$$

Thus also:

$$|J - sI| = |J^- - sI|$$

and we get the same characteristic equation for J and J^-.

3.4.2 Special equilibrium solutions

The unforced system ($F = G = 0$)

If our system is not forced from outside ($F = 0$, $G = 0$) we can see from eq. (3.6) to (3.9) that the system has a single equilibrium point which is the trivial solution $X = 0$, $Y = 0$, $Z = 0$. The stability behaviour of this special solution can be derived by linearizing eq. (2.4) at this point, which immediately leads to a completely decoupled system of differential equations:

$$\dot{X} = -aX \tag{3.12}$$

$$\dot{Y} = -Y \tag{3.13}$$

$$\dot{Z} = -Z. \tag{3.14}$$

We see that the linearized system has only dissipation terms left. The eigenvalues of the system there are $-a$, -1, -1 and the trivial solution represents a stable node.

The system without an oceanic-continental contrast

In the absence of an oceanic-continental contrast $G = 0$ the equilibrium solution derived from eq. (3.6) is:

$$X = F \tag{3.15}$$

$$Y = 0 \tag{3.16}$$

$$Z = 0, \tag{3.17}$$

and is located on the straight line given by eq. (3.15)-(3.17). So for a given F there exists only one equilibrium state. The stability behaviour of it can be found by applying eq. (3.15)-(3.17) to the Jacobian matrix J_e of eq. (3.10). We get:

$$J = \begin{pmatrix} -a & 0 & 0 \\ 0 & F-1 & -bF \\ 0 & bF & F-1 \end{pmatrix}. \tag{3.18}$$

Here we see that the variable X is decoupled and its eigenvalue is the constant systemparameter $-a$ independent from the forcing by F.

The characteristic equation of the matrix in eq. (3.18) has the form:

$$(s+a)[(s-F+1)^2 + (bF)^2] = 0 \tag{3.19}$$

and we get the eigenvalues:

$$s_1 = -a \tag{3.20}$$

$$s_{2,3} = F - 1 \pm jbF \tag{3.21}$$

$$\tag{3.22}$$

where $j = \sqrt{-1}$.

So we have one real and negative eigenvalue and two conjugate complex eigenvalues which depend on F. In figure 3.6 we see how the eigenvalues of

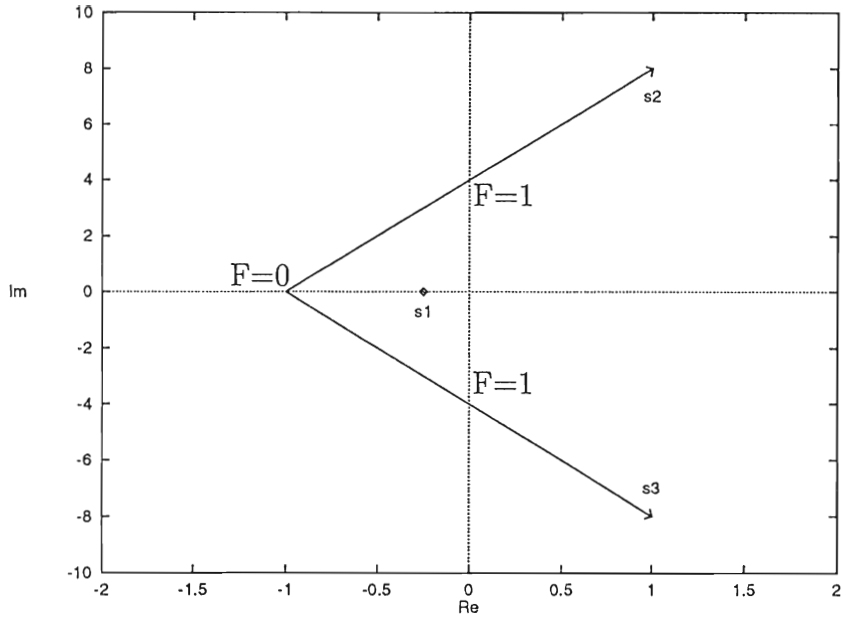

Figure 3.6: The behaviour of the eigenvalues by variation of F for the special path of equilibrium solutions $G = 0$, $X = F$, $Y = 0$, $Z = 0$.

the system change position in the complex plane by variation of F. Note that the eigenvalue s_1 has a fixed value and that the conjugate eigenvalues s_2 and s_3 move on a straight line through the points $-1, 0i$ and $0, \pm 4i$ in the complex plane.

For $F = 0$ we can verify our result from above for the trivial solution. For $0 < F < 1$ all real parts of the eigenvalues are negative. Hence for this range of F the solution trajectories will go to the equilibrium solution $F = X$ which is a stable focus. At $F = 1$ we have a Hopf bifurcation. The real parts of the conjugate complex eigenvalues change sign. For $F = 1$ we have a center and for $F > 1$ we get unstable foci.

3.4.3 Numerical bifurcation analysis

We have written a program in FORTRAN-77 which has the following algorithm:

- Calculates using eq. (3.9) $G(X, F)$ over a grid of points in X and F direction. This already can generate us the surface of equilibrium solution in the GFX-space.
- Calculates Y and Z from eq. (3.7) and (3.8). This can generate us the surface of the equilibrium solution in the XYZ-space.
- Calculates using eq. (3.10) the Jacobian matrix J_e at each equilibrium point.
- Solves for each Jacobian matrix corresponding to each equilibrium point the eigenvalue problem. For each point we get a triple of complex eigenvalues. This gives us information about the local stability of the solution at each equilibrium point.
- We separate the equilibrium points in groups, according to their stability. This allows us to plot the points on the surface with different colours according to their stability behaviour.

With this program we can generate a bifurcation analysis of the equilibrium solutions with two bifurcation parameters running. Thus we can get three dimensional plots by using one of the variables X, Y or Z and the two bifurcation parameters F and G. If we keep the bifurcation parameter F fixed we can also do a one-dimensional bifurcation analysis (see also [1]) in the G-X plane. Further we can also find out the stability of a single equilibrium point defined by the pair F and X.

From these plots we can get useful information about our system. For a given pair of parameters F and G we can:

- Find how many equilibrium points exist. (one or three)

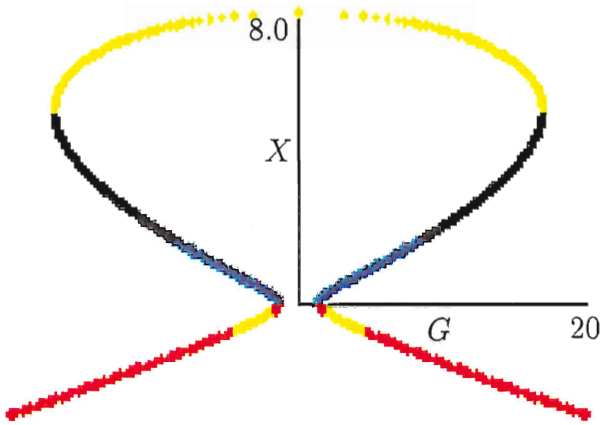

Figure 3.7: A one-dimensional bifurcation analysis using G representing the oceanic-continental contrast as the bifurcation parameter.

- Find what the stability behaviour of these points is.
- See if the equilibrium points will change their stability behaviour if we change slightly one or both bifurcation parameters. These can have big influence in the dynamical behaviour of our system.

A one-dimensional bifurcation analysis

Holding F constant we can do a bifurcation analysis of the equilibrium solutions using as the bifurcation parameter the oceanic-continental contrast G. In figure 3.7 we see a coloured version of the bifurcation analysis done by Houtekamer [1]. The bifurcation diagram is for $F = 8$. The horizontal axis is for the bifurcation parameter G while the vertical for the variable X. In the diagram G takes values more or less between -20 and 20 while X takes values between -3 and 8. Before we proceed we will make some definitions

which will help us to understand better the meaning of the colours plotted in the bifurcation diagrams. We have separated the equilibrium points in groups of the form:

$$n_1 S n_2 C$$

where S stands for Stable, C stands for Complex. n_1 gives the number of stable eigenvalues that is the number of eigenvalues with negative real part and can take the values $0, 1, 2$ or 3. n_2 gives the number of complex eigenvalues, that is the number of eigenvalues with non vanishing imaginary part. As complex eigenvalues can appear only as a conjugate pair n_2 can get only the values 0 or 2.

Example:
3S0C means that we have 3 stable eigenvalues and no conjugate complex eigenvalues. So these eigenvalues lie on the negative real axis. The colours have the following meaning:

- yellow - (unstable)
  One real part negative (not vanishing) and two positive (also not vanishing). Two eigenvalues are conjugate complex.
  Abbreviation: 1S2C

- black - (unstable)
  All real parts positive (not vanishing) Two eigenvalues are conjugate complex.
  Abbreviation: 0S2C

- blue - (unstable)
  Two real parts negative (not vanishing) and one positive (also not vanishing) Two eigenvalues are conjugate complex.
  Abbreviation: 2S2C

- red - (stable)
  All real parts are negative. Two eigenvalues are conjugate complex.
  Abbreviation: 3S2C

From the diagram we see that for the special case that $F = 8.0$ it is possible to have three or one equilibrium solutions. For $|G| < 1.367$ the system has only one equilibrium which is an unstable focus. For $|G| > 17.77$ we have again only one equilibrium solution which is a stable focus. In between, that is for $1.367 < |G| < 17.77$ we have three equilibrium solutions, which can have different stability behaviour as follows:

- two stable (3S2C) - one unstable (1S2C)
- all unstable, (two 1S2C and one 2S2C)
- one stable (3S2C) - two unstable (one 2S2C or 0S2C and one 1S2C)

This fact has a big influence on the dynamical behaviour of the system and plays also an important role in our investigation to find a chaotical region in the parameter space F and G.

From this picture we can see two Hopf-bifurcations which occur at the points where the equilibrium solution curve changes colour as follows:

1. from black to blue (0S2C to 2S2C)
2. from red to yellow (3S2C to 1S2C)

The latter is the most important one because here the equilibrium point changes from stable to unstable.

In fig. 3.8 we see four one-dimensional bifurcation diagrams for four different values of F. From the coloures in this four plots we can see that by increasing F from 0.5 to 8.0 new types of stability behaviour of the equilibrium arise.

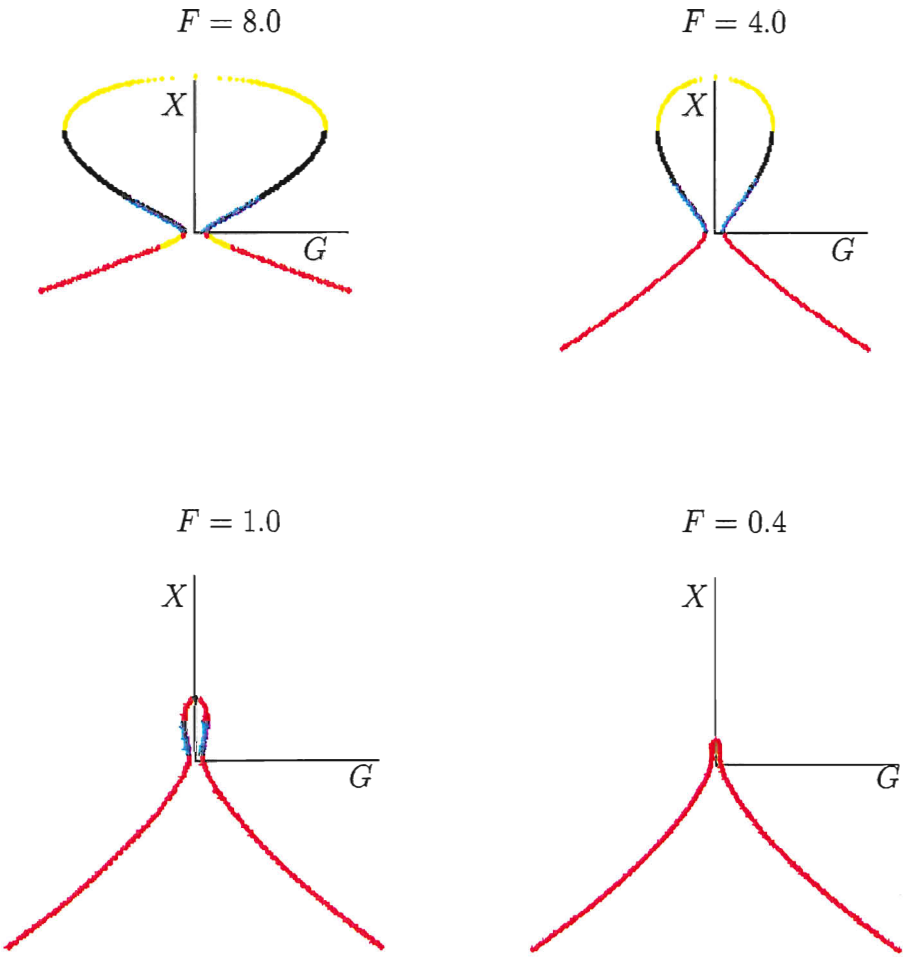

Figure 3.8: Four one-dimensional bifurcation diagrams for four different values of F representing the north-south gradients. The bifurcation parameter representing the oceanic-continental contrast is G.

A two-dimensional bifurcation analysis

If we take many one-dimensional bifurcation diagrams for different values of F and put them together in the direction of the F axis then we can get a two-dimensional bifurcation diagram. The surface of the a two-dimensional bifurcation diagram in the GFX-space is illustrated in figure 3.9. We can see that it passes through the origin and that it has a symmetry on the F-X plane. Because of the discretization and the plotting of coloured points in a three dimensional space, the surface is not very well visible, but if we imagine that the yellow lines on the top of the images belong to the top of the surface, the black and the blue lines to the middle part of the surface and the yellow on the right and the red lines to the bottom then we qualitatively can see what happens by changing the parameters. We also see that for large values of F a yellow area appears for negative X values. We also notice that the origin has a violet color because it is a stable node. The dark blue spot seen in the upper picture, at the point where the yellow upper surface is closest to the origin is the place in parameter space where the Hopf bifurcation is taking place for $F = X = 1.0$ and $G = 0$ in fig. 3.6. If we compare the colours of the line going through the origin and through this dark blue point then we see how the bifurcation of fig. 3.6 is visualised. The line is the upper bound of the two-dimensional bifurcation surface and represents a one dimenional bifurcation analysis for $F = X$ and and $G = 0$, see also [1] p.3-4.

We also observe that for large values of G the system has one stable equilibrium solution for negative values of X. So G stabilizes the system, but as $X < 0$ represents easterly winds this parameter area has no physical relevance.

We also can observe that for very small values of F we get stable equilibrium points.

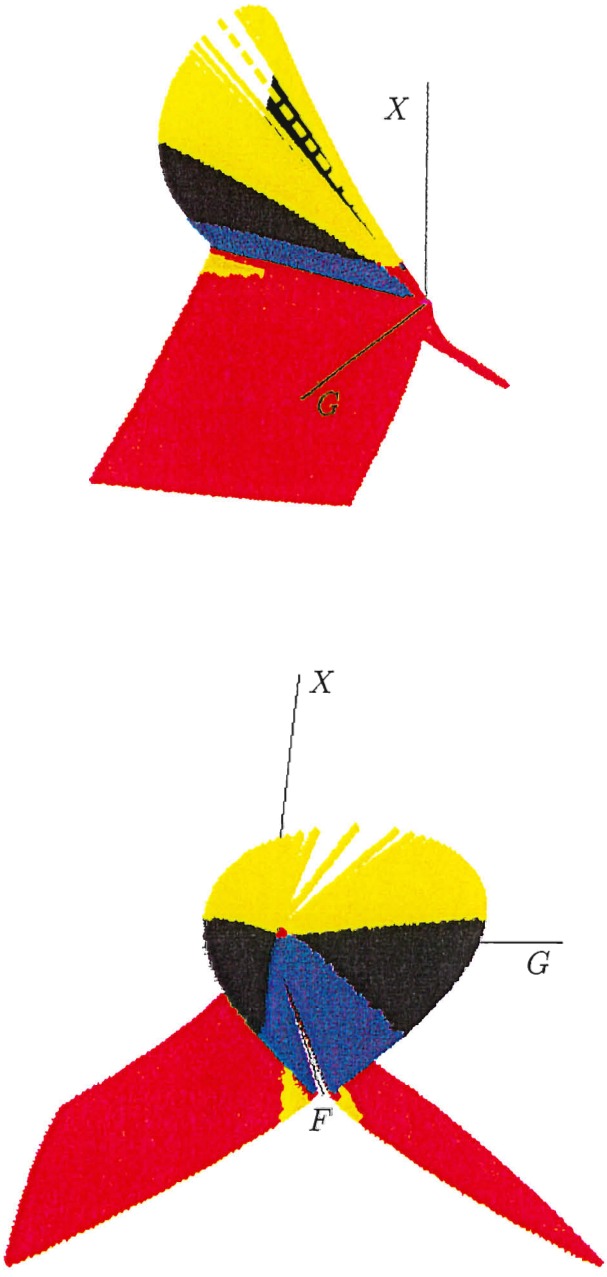

Figure 3.9: Two images of the two-dimensional bifurcation analysis from to different view points. F and G are the bifurcation parameters. The grid used is in the range: $0.0 \leq F \leq 8.0$,$-5.0 \leq X \leq 8.0$

3.5 Lyapunov stability of the system

In order to make conclusions about the stability and especially the global stability we use the following Lyapunov function:

$$V(X,Y,Z) = X^2 + Y^2 + Z^2 = R^2. \tag{3.23}$$

This simple function is positive definite and represents a sphere of radius R centered at the origin. The derivative:

$$\dot{V} = \frac{\partial V}{\partial X}\dot{X} + \frac{\partial V}{\partial Y}\dot{Y} + \frac{\partial V}{\partial Z}\dot{Z}$$

is in our case:

$$\frac{d(R^2)}{dt} = -\frac{1}{2}[a(2X - F)^2 + (2Y - G)^2 + (2Z)^2 - (aF^2 + G^2)] \tag{3.24}$$

If we set the right hand side of eq. (3.24) equal to zero it describes an ellipsoid, and has the form seen in picture 3.10. We can easily verify that this ellipsoid passes through the point $0,0,0$ since for this point the right hand side of eq. (3.24) is zero. Denote that the ellipsoid is shifted from the origin over a distance $\frac{F}{2}$ in the direction of the X-axis and $\frac{G}{2}$ in the direction of the Y-axis.

By testing the value of an arbitrary point which is not on the ellipsoid surface we conclude that the Lie derivative of the system is negative definite outside of the ellipsoid, vanishes on it and is positive inside of it.

If we thus define a sphere centered at (0,0,0) and completely enclosing the ellipsoid, and take any trajectorie outside of S we know that it will penetrate the sphere and remain inside of it [6]. Since also for $||\underline{x}|| \to \infty$, $V(\underline{x}) \to \infty$ we can say that the global flow will be attracted by the sphere. This means that our system is bounded and we can definitely say that as $t \to \infty$ the variables X,Y and Z will be in S.

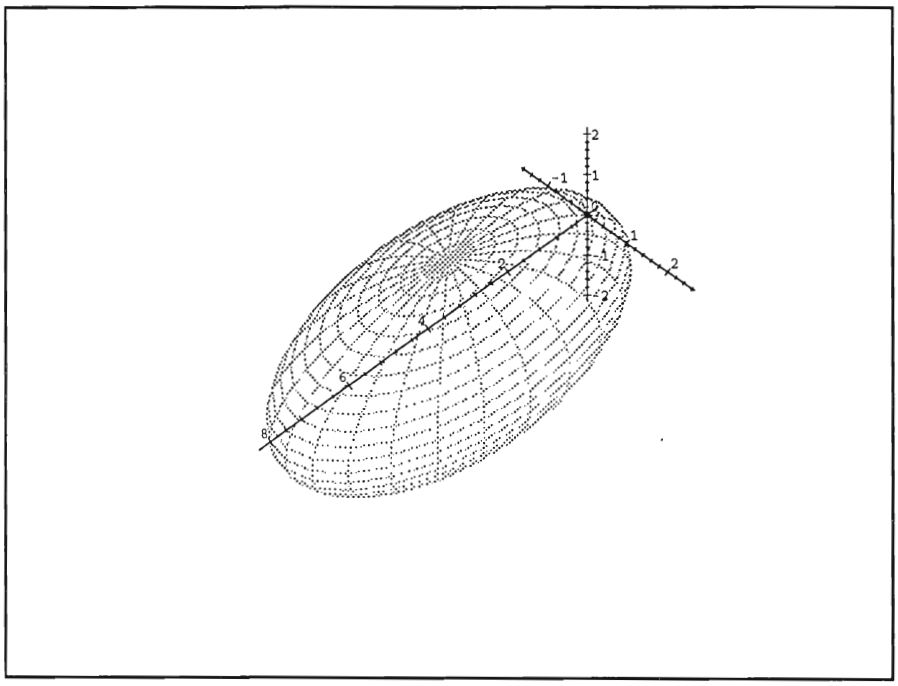

Figure 3.10: The ellipsoid surface gained from the Lyapunov function $V(X,Y,Z) = X^2 + Y^2 + Z^2$ for $F = 8.0$ and $G = 1.0$.

3.6 Lagrange-stability of the field

If we write eq. (1.1)-(1.3) in the general form:

$$\dot{\underline{x}} = \underline{f}(\underline{x}); \qquad \underline{x} \in \mathrm{R}^3 \underline{x}(0) = \underline{x}_0 \tag{3.25}$$

where the vector function $\underline{f}$ is given by

$$\underline{f}(\underline{x}) = (f_1(\underline{x}), f_2(\underline{x}), f_3(\underline{x})) \tag{3.26}$$

we can easily give the divergence of the vector field calculating the following

equation:

$$div = \frac{\partial f_1}{\partial X} + \frac{\partial f_2}{\partial Y} + \frac{\partial f_3}{\partial Z} \tag{3.27}$$

Hence the divergence of the vector field of the Lorenz model is

$$div = -a - 2 + 2X \tag{3.28}$$

So the time derivative of an infinitesimal volume-element V is:

$$\dot{V} = V div = -V(a + 2 - 2X) \tag{3.29}$$

We see that it would shrink for

$$X < 1 + \frac{a}{2}$$

This means that all the volume-elements, on trajectories of the system which are bounded under the plain

$$X = 1 + \frac{a}{2},$$

will end to attractors with zero volume.

Extending the Lorenz-84 equations (2.1)-(2.3) by equation (3.29) we get system:

$$\dot{X} = -Y^2 - Z^2 - aX + aF \tag{3.30}$$

$$\dot{Y} = XY - bXZ - Y + G \tag{3.31}$$

$$\dot{Z} = bXY + XZ - Z \tag{3.32}$$

$$\dot{V} = -V(a + 2 - 2X). \tag{3.33}$$

We are interested in integrating this system of four ordinary differential equations for the case where an attractor has regions of positive and negative divergence and follow the change of the volume V in time.

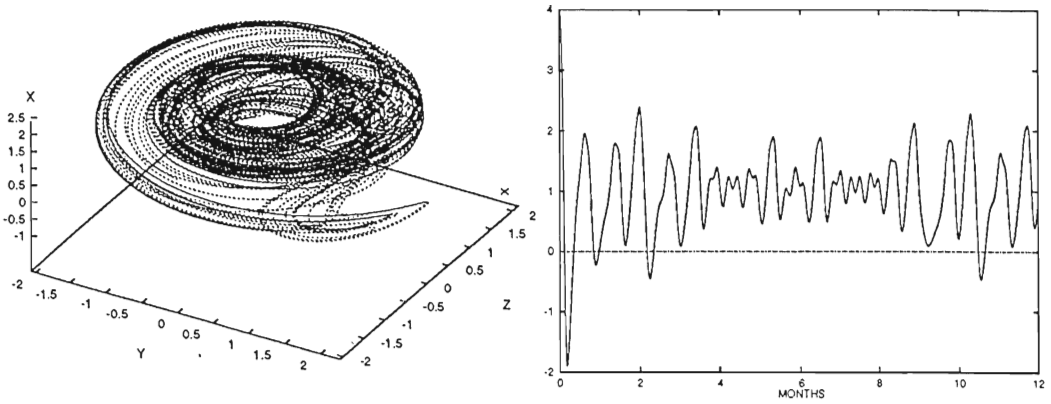

Figure 3.11: On the left the strange attractor for: $a = 0.25$, $b = 4.0$, $F = 8.0$, $G = 1.0$, $X_0 = 2.4$, $Y_0 = 1.0$, $Z_0 = 0.0$. On the right a plot of X versus time.

In fig. 3.11 we see the case of the strange attractor which definitely has a part in the region where X is greater than $1+\frac{a}{2} = 1.125$ and the divergence is positive. Despite of this fact we can see in fig. 3.12 where a time integration of the system (3.30)-(3.33) has been done, using the parameters $a = 0.25$, $b = 4.0$, $F = 8.0$, $G = 1.0$, $X_0 = 2.4$, $Y_0 = 1.0$, $Z_0 = 0.0$, that the volume may rise in the parts where the divergence is positive as for example in the beginning of the integration, but it rapidly approaches zero as soon as the trajectory visits for a while the region where the divergence is negative.

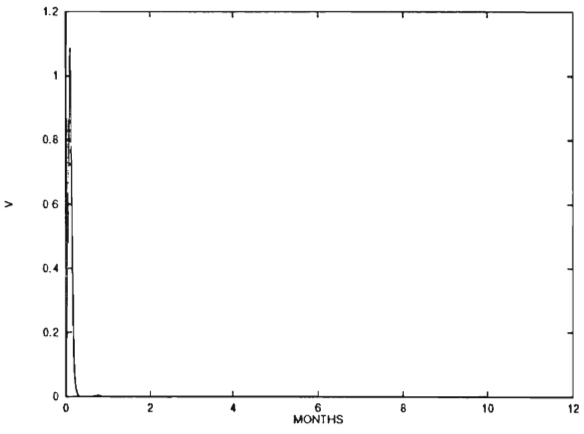

Figure 3.12: The evolution in time, of a small volume-element V for $a = 0.25$, $b = 4.0$, $F = 8.0$, $G = 1.0$, $X_0 = 2.4$, $Y_0 = 1.0$, $Z_0 = 0.0$,$V_0 = 0.1$

3.7 The Lyapunov exponents of the system

The Lyapunov exponents of the system eq. (2.1)-(2.3) can be determined using the algorithm described by Wolf et. al [15]. The Lyapunov exponents describe the mean rate of exponential divergence of initially neighboring trajectories. For a stable fixed point the Lyapunov exponents are just the real parts of the eigenvalues of the Jacobian matrix evaluated at the fixed point.

Generally a positive value denotes a divergence of the trajectories and thus a sensitive dependence of the system on initial conditions. Negative exponents denote convergence of the trajectories. A zero Lyapunov exponent corresponds to direction tangent to the flow.

For a three dimensional dynamical system, the following situations of Lyapunov spectra are possible:

- (-,-,-) ... fixed point or steady state solution,
- (0,-,-) ... limit cycle or periodic solution,
- (0,0,-) ... torus,
- (+,0,-) ... strange attractor.

In table 3.1 we have calculated some Lyapunov exponents for three different types of attractors found in the Lorenz-84 model.

We have used two Lyapunov exponent programs written by two different persons. Both of them use the Wolf algorithm. For both programs we found out that in the case of a fixed point the calculated Lyapunov exponents are actually the eigenvalues of the Jacobian matrix evaluated at the fixed point multiplied by a factor of $\ln 2$. For $F = 0.5$ and $G = 1.0$ the eigenvalues of the Jacobian matrix evaluated at the fixed point have been computed by an eigenvalue problem-solver.

F	G	$\lambda 1$	$\lambda 2$	$\lambda 3$	attractor
0.5	1.0	-1.197209769	-1.197209769	-1.995052786	fixed point
4.5	1.0	0.000198715	-0.095899931	-0.096623759	limit cycle
8.0	1.0	0.228140234	-0.000037541	-0.553264344	strange attractor

Table 3.1: The Lyapunov exponents for a fixed point ($F = 0.5$), a limit cycle ($F = 4.5$) and a strange attractor ($F = 8.0$).

They are:

$$\begin{aligned} s_1 &= -0.8299 + 1.6206j \\ s_2 &= -0.8299 - 1.6206j \\ s_3 &= -1.3830 \end{aligned} \tag{3.34}$$

We can easily verify that a multiplication of the Lyapunov exponents in the first row of table 3.1 by $ln2 \approx 0.69314$ gives the real parts of the eingenvalues s_1 to s_3. So one should be carefull by using the Wolf algorithm, if one wants to determine the exact eigenvalues of fixed points. The results should be multiplied by the factor ln 2. As we will see later in this work this observation has no influence in calculating the Kaplan-Yorke dimension of attractors using the Lyapunov exponents.

3.8 Lyapunov exponents in a system with competitive attractors

In nonlinear dynamics we often have the situation that a system has for certain parameters more than one positive attractor. Each attractor has his domain of attraction and we could say that it competes with the others in the state-space, in order to attract the surrounding trajectories. We speak about competitive attractors, [10]. We know from Lorenz [6] that he observed different types of attractors for the same parameters but slightly different initial

F	G	$\lambda 1$	$\lambda 2$	$\lambda 3$	attractor
6.0	1.0	-0.000040324	-0.091933386	-0.093591715	limit cycle
6.0	1.0	0.000857145	-0.350613345	-0.875247853	limit cycle

Table 3.2: The Lyapunov exponents for a system with competitive attractors. The only difference between the two calculations is the initial condition for the integration.

conditions and concluded by this that the system can have basin boundaries or separatrixes. Table 3.2 gives an example of two competitive limit cycles. The upper limit cycle has the initial condition $X_0 = 2.4$, $Y_0 = 1.0$, $Z_0 = 0.0$ while the other has $X_0 = 2.5$, $Y_0 = 1.0$, $Z_0 = 0.0$. The two limit cycles are shown in fig. 3.13.

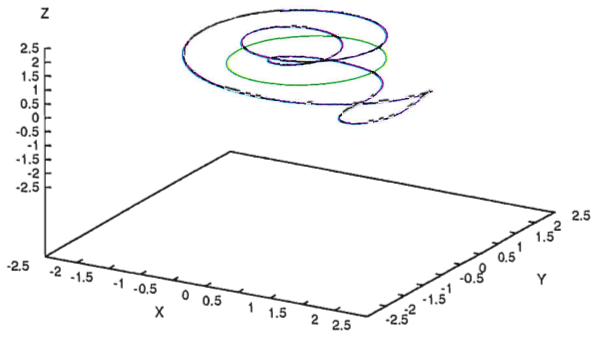

Figure 3.13: Two limitcycles in a system with competitive attractors.
$a = 0.25$, $b = 4.0$, $F = 6.0$, $G = 1.0$, $Y_0 = 1.0$, $Z_0 = 0.0$.
Green limitcycle: $X_0 = 2.4$, blue limitcycle: $X_0 = 2.5$

3.9 The Kaplan-Yorke-Dimension of the chaotic attractors

Mathematicians have developed different methods to define the dimension of attractors in nonlinear dynamics. One way to describe the dimension of an attractor is given in [12] and is called the Kaplan- Yorke dimension.

If we know the Lyapunov exponents of the attractor, we can easily calculate this dimension through the equation:

$$D_{KY} = j + \frac{\sum_{i=1}^{j} \lambda_i}{|\lambda_{j+1}|}, \tag{3.35}$$

where $\lambda_1 \geq \lambda_2 \geq \ldots \geq \lambda_n$ are the ordered Lyapunov exponents and j is the integer defined by the conditions:

$$\sum_{i=1}^{j} \lambda_i \geq 0, \sum_{i=1}^{j+1} \lambda_i < 0$$

In our case the possible dimensions are:

- fixed point ... 0,
- limit cycle ... 1,
- torus ... 2,
- strange attractor ... ≤ 3.

For table 3.1 we have calculated the corresponding Kaplan-Yorke dimensions D_{KY} which are given in table 3.3.

F	G	$\lambda 1$	$\lambda 2$	$\lambda 3$	D_{KY}
0.5	1.0	-1.197209769	-1.197209769	-1.995052786	0.000096599
4.5	1.0	0.000198715	-0.095899931	-0.096623759	1.002072109
8.0	1.0	0.228140234	-0.000037541	-0.553264344	2.412285187

Table 3.3: The Kaplan-Yorke dimensions D_{KY} corresponding to table 3.1.

3.10 The Correlation-dimension of the chaotic attractors

The Correlation-dimension [13] takes into account the regions of the attractor in which the system remains for the longest time. So if the system has a very inhomogeneous attractor, that is many regions are poorly visited, then the correlation dimension D_c will be much smaller than the Kaplan-Yorke dimension D_{KY}. This means that the correlation dimension D_c is from the dynamical point of view more relevant than the Kaplan-Yorke-Dimension D_{KY} [2].

The relation between the Correlation-dimension and the Kaplan-Yorke dimension is:

$$D_c \leq D_{KY} \tag{3.36}$$

The definition of the **Correlation-Dimension** (D_c) is:

$$D_c = \lim_{\epsilon \to 0} \frac{\log C(\epsilon)}{\log \epsilon}$$

where

$$C(\epsilon) = \frac{\sharp\{(x_i, x_j) \mid \|x_i - x_j\| < \epsilon\}}{N(N-1)}$$

Here we integrate our dynamical system in time and after the transient we take in constant time distances N points x_i on the attractor. We use any

Curve	F	G	D_c
(a)	0.5	1.0	0.000
(b)	4.5	1.0	1.029
(c)	8.0	1.0	2.289

Table 3.4: The parameters for three different attractors.

norm such as the euclidian or the maximum norm to define a measure for the distance between these points. Each pair of points which has distance smaller than ϵ is counted to $C(\epsilon)$. The correlation dimension is given by the slope of the curve

$$C(\epsilon) = f(\epsilon)$$

in a log-log plot as ϵ approaches zero.

In figure 3.14 we see such a plot obtained for $N = 40000$ and 41 different values of ϵ. The three curves (a), (b) and (c) correspond to three different parameters of F given in table 3.4.

For small values of F we get fixed points. The slope of the curve is zero and we get a horizontal line such as line (a). As F increases we come to a domain where limit cycles can appear. The dimension of a limit cycle is one and thus the slope is also one like in curve (b). In the chaotic regions we have taken the parameters $F = 8$, $G = 1.0$. From the slope of curve (c) we find the Correlation dimension 2.289. If we compare it with the Kaplan-Yorke dimension $D_{KY} = 2.41$ on table 3.3 for the same parameters and initial conditions, we see that eq. 3.36 is valid and that the chaotic attractor is slightly inhomogenous.

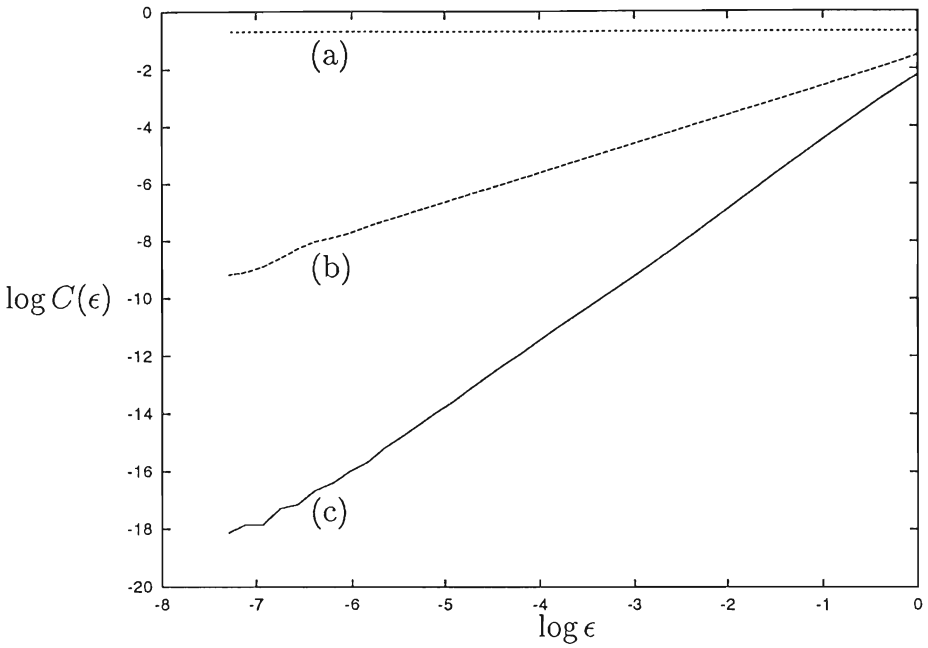

Figure 3.14: $\log C(\epsilon)$ vs. $\log \epsilon$ plot: (a) for a fixed point, (b) for a limit cycle and (c) for a strange attractor. The slopes are estimates for the Correlation-dimension D_c.

3.11 The influence of the parameters on the transient motion

In general we know that the timescale of the atmosphere is in the order of some weeks to some months. The LORENZ-84 model has in many cases of parameter pairs F and G and initial conditions X_0, Y_0 and Z_0 a transient motion in the order of this timescale. This is for example the case for $F = 6.5$ and $G = 1.2$ for which in figure 3.15 the atmospheric meridional temperature gradient X is plotted versus time.

But there are cases in the $F - G$ parameter space where the system behaves like having an extremely long timescale. After many longtime integrations with several parameters and initial conditions we came to the conclusion that the LORENZ-84 system can also have transient motions in the order of years

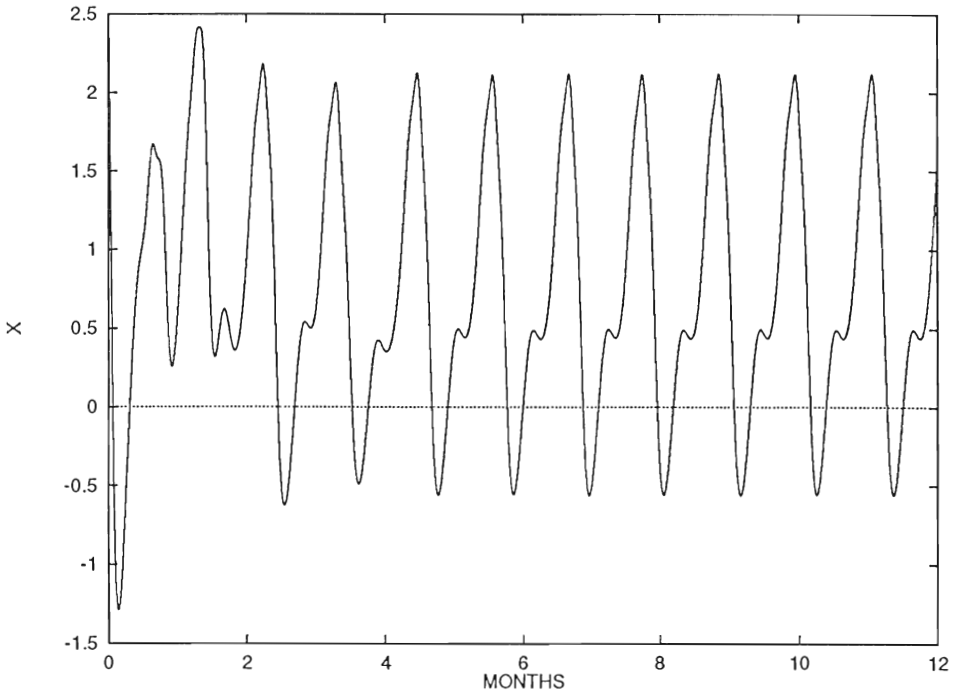

Figure 3.15: The transient motion for: $a = 0.25$, $b = 4.0$, $F = 6.5$, $G = 1.2$ takes the time of five months. The initial conditions where $X_0 = 2.5$, $Y_0 = 2.5$ and $Z_0 = 0.0$.

to decades.

For the parameters $F = 5.0$ and $G = 1.0$ for example we have taken as initial condition a cloud of points positioned on a three dimensional grid and observed their motion during a longtime integration. We observed that the transient motion of the points depends on the initial conditions and that it can be in some cases extremely long, that is in the order of $t = 3000$ to $t = 5000$ so about 40 to 70 years. After this extremely long time those points end on a simple limit cycle. For short time integrations the motion of the cloud appears to be chaotic.

During this long transient period the Poincaré sections have a fractal structure and integrations over a grid of 421 initial points in order to find the

Lyapunov exponents give us reason to believe that we have a system with competitive attractors consisting of a limit cycle and a strange attractor. So one should be very carefull in drawing conclusions about the system from the result of relatively short time integrations.

A very interesting phenomenon in comparing the Lyapunov exponent program and the Correlation dimension program for the parameters $F = 5.0$ and $G = 1.0$ is the following:

Integrating in time with our Runge-Kutta fourth order scheme using a time step h of 0.01 and the initial condition $X_0 = 5.0$, $Y_0 = 2.5$ and $Z_0 = 0.0$ we found the transient motion to be in the order of $t = 600$ or about 8 years. After that time the system came to a limit cycle.

A long time integration with the same values using the Lyapunov exponent program which starts evaluating the Lyapunov exponents after the $t = 5$, so before the transient motion is gone, gave as the result at $t = 5000$:

$$\lambda_1 = 0.18992, \lambda_2 = -0.04195, \lambda_3 = -0.41941$$

and a Kaplan-Yorke dimension D_{KY} of 2.3528. This is surprising since the Lyapunov exponent program had about the time of $t = 4400$ running on a limitcycle. Even more surprising was that for $t = 10000$ and $t = 25000$ as we can see in the first row of tabel 3.5 the Kaplan-Yorke dimensions were still far away from 1.0 which is the dimension of the limit cycle. So the convergence of the Lyapunov exponents and thus also the convergence of the Kaplan-Yorke dimension evolves very slowly and takes the time in the order of centuries. Apparently this transient effect has a overwhelming influence on the convergence of the Lyapunov exponents.

Using a Lyapunov exponent program which starts determining the Lyapunov exponents after the transient motion, at $t = 750$ we found a slight improvement in the convergence of the Lyapunov exponents. The Kaplan-Yorke dimensions are given in the second row of table 3.5.

For the same parameters and initial conditions we computed the Correlation dimension using 5000 points at a time distance of one time unit. We included

	$t = 5000$	$t = 10000$	$t = 25000$
Transient included	2.3528	2.1029	1.4496
Transient excluded	2.3006	1.9992	1.3236

Table 3.5: The Kaplan-Yorke dimensions calculated by a program which: (a) includes the transient motion and (b) waits until the system reaches the attractor, before it starts evaluating the Lyapunov exponents.

the initial transient motion in the data. The result was very positive for the reliability of the Correlation dimension program. In figure 3.16 we see the $\log C(\epsilon)$ vs. $\log \epsilon$ plot of the correlation dimension program. The slope of the linear part of the plot was found to be 1.01.

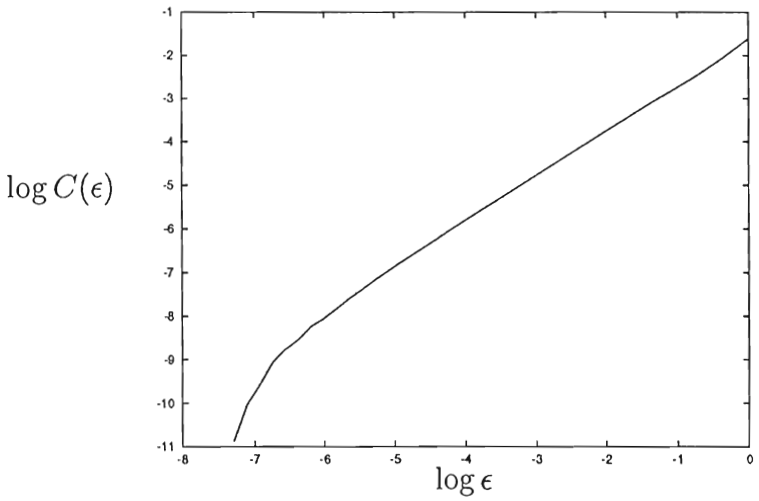

Figure 3.16: A $\log C(\epsilon)$ vs. $\log \epsilon$ plot for 5000 points and a total integration time $t = 5000$. Note that the transient motion was not deleted.

It is clear that one should start determining the Lyapunov exponents after the transient phase of the integration. This is especially true when determining the Kaplan-Yorke dimension. But as we observed the improvement of the convergence is not essential.

3.12 A chaotic region for the LORENZ-84 model

From the meteorological point of view it is very important to find the regions of the system where the behaviour is chaotic, as this is what happens with the atmosphere in nature. In order to find a domain in the F, G-parameter space with fully developed chaotic behaviour we have calculated for several pairs of these two parameters the Lyapunov exponents and the Kaplan-Yorke dimension for a large number of initial conditions. A similar investigation has been done in [8]. As initial conditions we have taken a huge grid of $21 \times 21 = 441$ points on the $Z = 0$ plane within the range $-5 \leq X \leq +5$ and $-5 \leq Y \leq +5$ and a discretization of 0.5 between two points. The integration scheme was RUKU fourth order with the time step h of 0.01. The total integration time was in the order of 140 years, so extremely long compared to the usual time scale of the atmosphere.

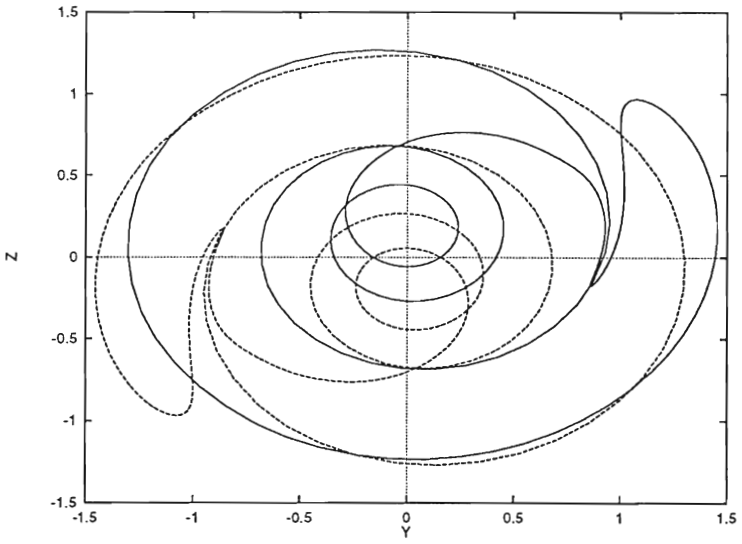

Figure 3.17: Projection of a limit cycle in the YZ-plane and its symmetrical solution. The continued line is the limit cycle for X, Y, Z, G, F. The dashed line gives the limit cycle for $X, -Y, -Z, -G, F$.

Parameters	$F = 7.5$	$F = 8.0$	$F = 8.5$	$F = 9.0$	$F = 9.5$
$G = 0.9$	$D_{KY} = 1.00$	$D_{KY} = 2.37$	$D_{KY} = 1.00$	$D_{KY} = 1.00$	$D_{KY} = 1.00$
$G = 1.0$	$D_{KY} = 1.00$	$D_{KY} = 2.42$	$D_{KY} = 2.26$	$D_{KY} = 1.00$	$D_{KY} = 1.00$
$G = 1.1$	$D_{KY} = 2.38$	$D_{KY} = 2.42$	$D_{KY} = 2.24$	$D_{KY} = 1.00$	$D_{KY} = 1.00$
$G = 1.2$	$D_{KY} = 2.14$	$D_{KY} = 1.00$	$D_{KY} = 1.00$	$D_{KY} = 1.00$	$D_{KY} = 1.00$
$G = 1.3$	$D_{KY} = 1.00$	$D_{KY} = 2.35$	$D_{KY} = 2.28$	$D_{KY} = 2.10$	$D_{KY} = 1.00$
$G = 1.4$	$D_{KY} = 0.00$	$D_{KY} = 0.00$	$D_{KY} = 1.00$	$D_{KY} = 2.11$	$D_{KY} = 1.00$

Table 3.6: A domain in the parameter space $F - G$ with chaotic behavior. The integration time $t = 10000$ corresponds to approximately 137 years.

The fact that our dynamical system eq. (2.1)-(2.3) has symmetrical solutions simplifies our investigation very much. If $(X(t), Y(t), Z(t), G, F)$ is a solution of eq. (2.1)-(2.3) then $(X(t), -Y(t), -Z(t), -G, F)$ is also a solution of the system. Thus if we find all the attractors the system has for specific values of G and F, we also found all the attractors the system has for the values $-G$ and F. The latter attractors in the X, Y, Z- space will be symmetrical about the X-axis to the first. So no investigation for the pairs $-G, F$ are necessary if we know the results for G, F.

In figure 3.17 we see from the YZ-projection of the phase portrait the symmetry of attractors for G, F and $-G, F$. Here we see a limit cycle (solid line) for X_0, Y_0, Z_0, G, F and its symmetrical limit cycle (dashed line) for $X_0, -Y_0, -Z_0, -G, F$.

In table 3.6 we show the Kaplan-Yorke dimension of the attractors found as a function of F and G for a small window in parameter space.

Special remarks about the table: For $F = 7.5$, $G = 1.0$, $F = 8.5$, $G = 0.9$ and $F = 9.0$, $G = 1.2$ we get a weak stable limit cycle and the convergence of the Kaplan-Yorke dimension evolves very slowly. Even after $t = 40000$ or about 550 years many integrations of the 421 initial points give in each case Kaplan-Yorke dimensions close to but not exactly 1.00.

Definitely there are chaotic windows in the parameter space. We assume, but we can not guarantee due to the discretization, that there is a small chaotic window in the region $8.0 \leq F \leq 8.5$ and $1.0 \leq G \leq 1.1$, which could be extended for the practical use to $7.5 \leq F \leq 8.5$ and $1.0 \leq G \leq 1.1$ as the transient motion for $F = 7.5$ and $G = 1.0$ is extremely long and irregular.

We also remark that despite of the weak convergence of the Lyapunov exponent program in some cases, we did not use the Correlation dimension program although we have seen its reliability for such cases, because the calculation time for the latter is very long.

Chapter 4

Discussion

We have observed that even though the Lorenz-84 atmospheric model looks very simple it shows a variety of interesting dynamical phenomena. Very special in the investigations was the sensitivity of the system to parameter variations and the complexity of the attractors found in it. Fixed points, simple limit cycles, higher subharmonic limit cycles and chaotic attractors have been found. We observed that the system shows regular behaviour for low values of forcing (F, G) and that the irregular behaviour appears for larger values of the forcing terms and comes in windows in the parameter space.

In section 3.4.1 we mention the symmetry properties of the equilibrium solution and also the symmetry of the stability behaviour for positive and negative G.

From our one and two dimensional bifurcation analysis of the equilibrium solutions in section 3.4.3 we have observed a variety of stable and unstable equilibrium solutions which will have a large influence on the dynamical behaviour of the system. One should always have the diagrams in mind when searching for a chaotic region.

In section 3.5 we have shown that the global flow of the system is bounded

and remains within a sphere centered at the origin. In section 3.6 we saw that we can separate the state-space by the plane $X = 1 + \frac{a}{2}$ in a domain with positive and a domain with negative divergence. Attractors which go through both domains seem to end to zero volume when t goes to infinity.

In section 3.7 we warn the reader that the Wolf algorithm gives for fixed point attractors not exactly the real parts of the Jacobian matrix evaluated at the fixed point. The factor $\ln 2$ should be multiplied to the result. If this factor is also found in calculations of limit cycles and strange attractors we remark that it has no influence in the calculation of the Kaplan-Yorke dimension if we see eq. (3.35) in section 3.9. In section 3.8 we have seen that competitive attractors are possible. In our various integrations we have observed only coexistence of limit cycles, but not coexistence of a strange attractor and a limit cycle or other combinations.

In section 3.9 and 3.11 we experienced that long integration times greater than $t = 10000$ are necessary in order to determine the Kaplan-Yorke dimension of attractors accurate enough . Sometimes when we have weak limit cycles even $t = 40000$ which corresponds to five and a half centuries is not enough time for the Lyapunov exponents to converge. The Kaplan-Yorke dimension of chaotic attractors was in general between 2.10 and 2.42, depending on the parameters. As we have noticed, starting evaluating the Lyapunov exponents on the attractor, that is after the transient motion, improves slightly the convergence of the Lyapunov exponents but the following question is for us still open: How could the algorithm to determine the Lyapunov exponents be improved in order to get faster convergence and thus reduce the calculation time?

In section 3.10 we experienced that the chaotic attractors are slightly inhomogenous by comparing the Correlation dimension with the Kaplan-Yorke dimension. A number of 40000 points on the attractor is recommended for a very good approximation of the Correlation dimension. The disadvantage of the Correlation dimension program is that it needs a long time to integrate comparing it to the Lyapunov exponent program.

In section 3.11 we observed that the system can have extremely long transient motion behaviour for some cases in the parameter space. Here one must do long time integrations to observe whether or not the attractor goes to a limit cycle or to a chaotic attractor. We still do not know what the exact explanation of this long transient effect is, when it occurs and which attractors (stable and unstable) are involved in this effect.

In the previous section 3.12 we have investigated a chaotic regime in the FG-parameter space. We have seen that it is not easy to find a chaotic region over a large range of parameters and the relevant questions would be: Is it possible that we could find better chaotic regions with larger windows of irregular behaviour in the time dependent problem?

We also mention that because of symmetry properties of the system, explained in section 3.12, table 1 in [8] should be symmetric for positive and negative values of G. Also because of the long transient behaviour of the system for some parameters, discussed in section 3.11, we have to correct table 1 in [8] for the cases $F = 5.0$, $G = 1.0$ and $F = 8.0$, $G = 1.2$, since after the transient motion the system has converged to a limit cycle. We also have to correct the case $F = 6.0$, $G = 1.0$ of the same table where according to section 3.8, two competitive limit cycle attractors are observed in the system. This is also verified by calculations of Lorenz in [6] p.381.

We also warn the reader from the typing error in page 3, eq. (4) of the [1] paper. There eq. (4) should have the form:

$$Y = \frac{(1-X)G}{(1-2X+(1+b^2)X^2)}.$$

Finally we assume that there are still many effects in the Lorenz-84 atmospheric model which would be worthwhile to investigate. An interesting question would be: What types of bifurcations are involved in the transition to chaos in this model?

Bibliography

[1] *P. HOUTEKAMER* : An analysis of the Lorenz-1984 equations. *Research Department of Mathematics - State University Utrecht* (1989).

[2] *G.H.M. VAN DER HEIJDEN* : Nonlinear Drillstring Dynamics a quest for the origin of chaotic vibrations. *Faculteit Wiskunde en Informatica - State University Utrecht, dissertation.* (1994).

[3] *E.N. LORENZ* : Irregularity: A fundamental property of the atmosphere. *Tellus 36 A* (1984), p.98-110.

[4] *E. DOEDEL* : Auto: Software for continuation and bifurcation problems in ordinary differential equations. *California Institute of technology, Pasadena, California* (1986).

[5] *J. LA SALLE and S. LEFSCHETZ* : Die Stabilitätstheory von Ljapunow. *BI-Hochschultaschenbuch 194* (1967).

[6] *E.N. LORENZ* : Can chaos and intransitivity lead to interannual variability? *Tellus 42 A* (1990), p.378-389.

[7] *E. BIRCHFIELD* : A coupled ocean-atmosphere climate model: temperature versus salinity effects on the thermohaline circulation. *Springer-Verlag* , (1989).

[8] *P.J. ROEBBER* : Climate variability in a low-order coupled atmosphere-ocean model. *Department of Atmospheric Science State University of New York at Albany Albany, New York* (1994).

[9] *H. POINCARÉ* : Mémoire sur les courbes définies par les équations différentielles I-VI. *Oeuvre I. Gauthier - Villars, Paris* (1880-90).

[10] *J.M.T. THOMPSON and H.B. STEWART* : Nonlinear Dynamics and Chaos. *John Wiley and Sons, Chichester, New York* (1986).

[11] *W.H. STEEB and A. KUNICK* : Chaos in dynamischen Systemen. *Wissenschaftsverlag Mannheim* (1989).

[12] *J.L. KAPLAN and J.A. YORKE* : Chaotic behavior of multidimensional difference equations, in *Functional Differential Equations and Approximation of Fixed Points H.-O. Peitgen, H.-O. Walther (eds.) , Lecture Notes in Mathematics 730, Springer-Verlag, New York,*(1984), p.204-227.

[13] *P. GRASSBERGER, I. PROCACCIA* : *Measuring the strangeness of strange attractors Physica 9D,*(1983), p.189-208.

[14] *F. VERHULST* : *Nonlinear differential Equations and dynamical Systems. Springer Verlag,*(1990).

[15] *A. WOLF, J.B. SWIFT, H.L. SWINNEY and J.A. VASTANO* : *Determining Lyapunov exponents from a time series. Physica 16D,*(1985), p.285-317.

[16] *M.K. JAIN, S.R.K. Iyengar and R.K. JAIN*: *Numerical Methods for Scientific and Engineering Computaion. Wiley Eastern Limited,*(1985).

Overzicht recente KNMI-publikaties

KNMI-PUBLIKATIES MET NUMMER:

150-27. Klimatologische gegevens van Nederlandse stations: normalen en extreme waarden van de 15 hoofdstations voor het tijdvak 1961-1990 / samenst. H.J. Krijnen en J.W. Nellestein. 1992
165-5. Historische weerkundige waarnemingen:beschrijving antieke meetreeksen / H.A.M.Geurts en A.F.V.van Engelen. 1992
172. Vliegen in weer en wind : geschiedenis van de luchtvaartmeteorologie / Tj. Langerveld. 1988
173. Werkdocument verspreidingsmodellen / Red. H. van Dop; in samenwerking met het RIVM. 1988
174. Ons klimaat, onze planeet / voorw. H. Tennekes; inleiding C.J.E. Schuurmans; met bijdr. van H. van Dop ea. 1989
175. Klimaat-onderzoek Westland ten behoeve van kustuitbreiding / W.H. Slob. 1989
176. Stormenkalender : chronologisch overzicht van alle stormen (windkracht 8 en hoger) langse de Nederlandse kust voor het tijdvak 1964-1990 / B. Augustijn, H. van Daan, B. van Mourik, D. Messerschmidt en B. Zwart. 1990
177. Description of the RIVM puff dispersion model / G.H.L. Verver, F.A.A.M. de Leeuw, H.J. Rheineck-Leyssius. 1990
178. Modules Bureau Vorming en Opleiding **(uitsluitend intern beschikbaar;** lijst op aanvraag). 1991- .
179. Catalogus van aardbevingen in Nederland / G. Houtgast. 1991
179[a]. idem, 2e gewijzigde druk. 1992
180. List of acronyms in environmental sciences / [P.Geerders]. 1991
180[a]. List of acronyms in environmental sciences:revised edition / [P.Geerders and M. Waterborg] 1995
181. Nationaal gebruik van de groepen 7wwW1W2 en 960ww voor landstations / [samenst. H. van Drongelen, A. Kamphuis en P.Y. de Vries] 1992
182. Wijzigingen aeronautische codes : 1 juli 1993 / [P.Y. de Vries en A.A.Brouwer] 1993
183. [verschijnt medio 1995]
184. Inleiding tot de algemene meteorologie / B. Zwart, A. Steenhuisen m.m.v. H. Krijnen 1994
185. Handleiding voor het gebruik van sectie 2 van de FM-13X SHIP code door stations op zee / KNMI, KL, KM 1994
185[a]. Handleiding voor het gebruik van sectie 2 van de FM13-X SHIP-code voor waarnemers op zee / KNMI, KL, KM 1995
(-) Zonnestraling in Nederland / C.A. Velds (uitg.Thieme in de serie Het klimaat van Nederland; dl. 3) 1992

WETENSCHAPPELIJKE RAPPORTEN:

88-01 Central Sudan surface wind data and climate characteristics/ E.H. ABu Bakr.
88-02 Stratocumulus modeling / P.G. Duynkerke.
88-03 Naar een niet-linear wateropzetmodel : stand van zaken februari 1988 / C.J. Kok.
88-04 The boundary layer wind regime of a representative tropical African region, central Sudan / E.H. ABu Bakr.
88-05 Radiative cooling in the nocturnal boundary layer / S.A. Tjemkes.
88-06 Surface flux parameterization schemes : developments and experiences at KNMI/A.A.M.Holtslag and A.C.M. Beljaars.
89-01 Instability mechanisms in a barotropic atmosphere / R.J. Haarsma.
89-02 Climatological data for the North Sea based on observations by voluntary observing ships over the period 1961-1980 / C.G. Korevaar.
89-03 Verificatie van GONO golfverwachtingen en van Engelse fine-mesh winden over de periode oktober 1986 - april 1987 / R.A. van Moerkerken.
89-04 Diagnostics derivation of boundary layer parameters from the outputs of atmospheric models / A.A.M. Holtslag and R.M. van Westrhenen.
89-05 Statistical forecasts of sunshine duration / Li Zhihong and S. Kruizinga.
90-01 The effect of a doubling atmospheric CO2 on the stormtracks in the climate of a general circulation model / P.C. Siegmund.
90-02 Analysis of regional differences of forecasts with the multi-layer AMT-model in the Netherlands / E.I.F. de Bruin, Li Tao Guang and Gao Kang.
90-03 Description of the CRAU data-set : Meteosat data, radiosonde data, sea surface temperatures : comparison of Meteosat and Heimann data / S.H. Muller, H. The, W. Kohsiek and W.A.A. Monna.
90-04 A guide to the NEDWAM wave model / G. Burgers.
91-01 A parametrization of the convective atmospheric boundary layer and its application into a global climate model / A.A.M. Holtslag, B.A. Boville and C.H. Moeng.
91-02 Turbulent exchange coefficients over a Douglas fir forest / F.C. Bosveld.
92-01 Experimental evaluation of an arrival time difference lightning positioning system / H.R.A.Wessels.
92-02 GCM control run of UK Met.Off. compared with the real climate in the NW European winter / J.J. Beersma.
92-03 The parameterization of vertical turbulent mixing processes in a GCM of the Tropical Pacific / G.Janssen.
92-04 A scintillation experiment over a forest / W.Kohsiek.
92-05 Grondtemperaturen / P.C.T.van der Hoeven en W.N.Lablans
92-06 Automatic supression of anomalous propagation clutter for noncoherent weather radars / H.R.A. Wessels and J.H. Beekhuis.
93-01 Searching for stationary stable solutions of Euler's equation / R. Salden.
93-02 Modelling daily precipitation as a function of temperature for climatic change impact studies / A.M.G. Klein Tank and T.A. Buishand.
93-03 An analytic conceptual model of extratropical cyclones / L.C. Heijboer.
93-04 A synoptic climatology of convective weather in the Netherlands / Dong Hongnian.
93-05 Conceptual models of severe convective weather in the Netherlands / Dong Hongnian.
94-01 Seismische analyse van aardbevingen in Noord-Nederland : bijdrage aan het multidisciplinaire onderzoek naar de relatie tussen gaswinning en aardbevingen / H.W.Haak en T. de Crook.
94-02 Storm activity over the North Sea and the Netherlands in two climate models compared with observations / J.J.Beersema.
94-03 Atmospheric effects of high-flying subsonic aircraft / W. Fransen.
94-04 Cloud-radiation-hydrological interactions : measuring and modeling / A.J. Feijt, R. van Dorland, A.C.A.P. van Lammeren, E. van Meijgaard and P. Stammes.
94-05 Spectral ultraviolet radiation measurements and correlation with atmospheric parameters / F. Kuik and H. Kelder
95-01 Transformation of precipitation time series for climate change impact studies/A.M.G.Klein Tank and T.A.Buishand
95-02 Internal variability of the ocean generated by a stochastic forcing / M.B.H. van Noordenburg
95-03 Applicability of weakly nonlinear theory for the planetary-scale flow / E.A. Kartashova
95-04 Changes in tropospheric NOx and O3 due to subsonic aircraft emissions / W.M.F. Wauben, P.F.J. van Velthoven and H. Kelder
95-05 Numerical studies on the Lorenz-84 atmosphere model / Leonardo Anastassiades

TECHNISCHE RAPPORTEN:

103a. Wind-chill / B. Zwart. Geheel herz.ed. 1992
105. Description of the Cabauw turbulence dataset 1977-1979 / C. Hofman. 1988
106. Automatische detektie van inversies met sodar / A.C.M. Beljaars en R. Agterberg. 1988
107. Numerieke atmosfeermodellen / A.P.M. Baede. 1988

108. Inpassingen van Meteosat informatie in de meteorologische besluitvorming / J. Roodenburg. 1988
109. Opmeting van het aardmagneetveld in Nederland, herleid naar 1985 / J.H. Rietman. 1988
110. Crau 1987 : the KNMI contribution / W. Kohsiek, J.G. van der Vliet and W.A.A. Monna. 1988
111. Van Penman naar Makkink : een nieuwe berekeningswijze voor de klimatologische verdampingsgetallen / red. J.C. Hooghart en W.N. Lablans. 1988
112. Description of a software library for the calculation of surface fluxes / A.C.M. Beljaars, A.A.M. Holtslag and R.M. van Westrhenen. 1989
113. Menghoogteberekeningen voor het Europees continent:een vergelijkend onderzoek / M.P. Scheele en H. van Dop. 1989
114. Operational WAMS statistics over the period December 1986 - March 1987 / R.A. van Moerkerken, C.J. Komen and P.A.E.M. Janssen. 1989
115. Mesoscale terrain roughness mapping of the Netherlands / R. Agterberg and J. Wieringa. 1989
116. Geschiedenis van de landbouwmeteorologie in Nederland tot 1972 / J.P.M. Woudenberg. 1989
117. Instabiliteiten rond de straalstroom / R.P. Henzen. 1989
118. Verificatie van GONO golfverwachting over de periode oktober 1987- april 1988 / R.A. van Moerkerken. 1989
119. Spectra en gradiënten van hoge windsnelheden te Cabauw tot 200m / R.W.M. Meijer. 1989
120. About the possibilities of using an air tranformation model in Taiyun, Shanxi province, China / J. Reiff, Li Tao-Guang and Gao Kang. 1990
121. The effect of wave data assimilation of the numerical simulation of wave energy advection/ M.de la Heras and G.Burgers 1990
122. Objective analysis of precipitation observations during the Chernobyl episode/M.P.Scheele and G.H.L.Verver. 1990
123. The use of satellite data in the ECMWF analysis system / K. Lablancz. 1990
124. A primitve equation model for the Equatorial Pacific / M.A.F. Allaart and A. Kattenberg. 1990
125. Technical description of the high-resolution air mass transformation model at KNMI / E.I.F. de Bruin and A.A.M. Holtslag 1990
126. Verificatie kwantitatieve neerslagverwachting korte termijn (proefperiode) voor 5 regio's / D. Messerschmidt.1990
127. Quantitative processing of Meteosat-data : implementation at KNMI : applications / S.H. Muller. 1990
128. A primary experiment of statistical interpolation scheme used in sea waves data assimilation / Gao Quanduo. 1990
129. Coordinate conversions for presenting and compositing weather radar data / H.R.A. Wessels. 1990
130. Flux-profile relationships in the nocturnal boundary layer / P. Bouwman 1990
131. The implementation of the WAQUA/CSM-16 model for real time storm surge forecasting / J.W.de Vries 1991
132. De luchttemperatuur op West-Ameland / F. Ynsen. 1991
133. Seizoenverloop en trend in de chemische samenstelling van de neerslag te Lelystad/T.A.Buishand en J.H.Baard. 1991
134. Technical description LAM and OI : Limited Area Model and Optimum Interpolation Analysis / W.C. de Rooy and L.M. Hafkenscheid. 1991
134a. Idem. Second ed. 1992
135. Relative trajectoriën in en rond een depressie / J.P.A.J. van Beeck. 1991
136. Bepaling van een directe en diffuse straling en van zonneschijnduur uit 10-minuutwaarden van de globale straling / W.H. Slob en W.A.A. Monna. 1991
137. LAM en NEDWAM statistics over the period October 1990 - April 1991 / R.A. van Moerkerken. 1991
138. Dagsom van de globale straling : een rekenmethode en verwachtingsverificatie / M.C. Nolet. 1991
139. A real-time wave data quality control algorithm / Maria Paula Etala. 1991
140. Syllabus Fysische Meteorologie I / H.R.A. Wessels. 1991
141. Systeembeschrijving Mist Voorspel Systeem MIVOS / D. Blaauboer, H.R.A. Wessels en S. Kruizinga. 1992
142. Het nachtelijk windmaximum : een interactive verwachtingsmethode / N. Maat en H. Bakker. 1992
143. Neerslagverificatie LAM / W.C.de Rooy en C.A. Engeldal †. 1992
144. Aanpassing vocht-bedekkingsgraadrelaties in het LAM / W.C. de Rooy. 1992
145. Een verificatie van de Eurogids, de gidsverwachting voor vervoer en toerisme / H.G. Theihzen. 1992
146. The earth radiation budget experiment: overview of data-processing and error sources / Arnout J. Feijt 1992
147. On the construction of a regional atmospheric climate model / Jens H. Christensen and Erik van Meijgaard 1992
148. Analyse van torenwindgegevens over het tijdvak 1977 tot en met 1991 / Gertie Geertsema 1992
149. The performance of drag relations in the WAQUA storm surge model / J.R.N. Onvlee. 1993
150. Verification of 3I retrievals vis-a-vis radiosonde observations / G.J. Prangsma. 1993
151. Het Synoptisch Symposium 1992: een verslag / red. H.G.Theihzen. 1993
152. The Aciforn hydrological programme : the water cycle of a Douglas fir forest / F.C. Bosveld ...[et al.]. 1993
153. Het APL+ programma / R.M. van Westrhenen. 1993
154. The effect of spatial averaging on threshold exceedances of daily precipitation amounts / T.A. Buishand, B. van Mourik and A.M.G. Klein Tank. 1993
155. Neerslagvergelijking van Espelo ten opzichte van het omgevingsgemiddelde / J.P.M. van Dun en J. Verloop. 1993
156. On the effetcs of limited spectral resolution in third-generation wave models/I.V.Lavrenov and J.R.A.Onvlee. 1993
157. Meteorologische evaluatie van de zichtmetingen langs de A16 / H.R.A. Wessels. 1993
158. Het programma voor berekening van zonneschijnduur uit globale straling / U. Bergman. 1993
159. Verificatie weersverwachtingen 1955-1993 / H. Daan. 1993
160. Drie objectieve indices voor clear-air turbulence nader bekeken / H. Bakker. 1993
161. The ASGASEX experiment / W.A. Oost. 1994
162. TEBEX observations of clouds and radiation -potential and limitations / P. Stammes, A.J. Feijt, A.C.A.P. van Lammeren and G.J. Prangsma. 1994
163. Evaluatie kwaliteitsonderzoek mistdata "Mistprojekt A-16" Breda / M. van Berchum. 1994
164. Standaard stralingsmetingen met een zonnevolger / A.C.A.P. van Lammeren en A. Hulshof. 1994
165. Neurale netwerken versus lineaire regressie : een onderzoek naar de waarde van neurale netwerken in de meteorologische praktijk / R.M. Meuleman 1994
166. Seismische analyse van de aardbeving bij Alkmaar op 6 augustus 1994 / [afdeling Seismologie] 1994
167. Seismische analyse van de aardbeving bij Alkmaar op 21 september 1994 / [afdeling Seismologie] 1994
168. Analyse van het seismische risico in Noord-Nederland / Th. de Crook, B. Dost en H.W. Haak 1995
169. Evaluatie van neerslagprognoses van numerieke modellen voor de Belgische Ardennen in december 1993 / Erik van Meijgaard. 1994
170. DARR-94 / C.P.G. Lomme 1994
171. EFEDA-91: documentation of measurements obtained by KNMI / W.A.A. Monna, W. Kohsiek, G.J. Prangsma, J.N. Roozekrans and J.G. van der Vliet. 1994
172. Cloud lidar research at the Royal Netherlands Meteorological Institute and KNMI2B2 version 2 cloud lidar analysis software documentation / Alexandre Y. Fong and Andre C.A.P. van Lammeren 1994
173. Measurement of the structure parameter of vertical wind-velocity in the atmospheric boundary layer / R. van der Ploeg 1995
174. Report of the ASGASEX'94 workshop / ed. by W.A. Oost 1995
175. Over slecht zicht, bewolking, windstoten en gladheid / J. Terpstra 1995